Physics potential of searching for 0νββ decays in JUNO *

Jie Zhao(赵洁)[1;1)] Liang-Jian Wen(温良剑)[1,2;2)] Yi-Fang Wang(王贻芳)[1,2] Jun Cao(曹俊)[1,2]

[1] Institute of High Energy Physics, Chinese Academy of Sciences, Beijing 100049, China
2 State Key Laboratory of Particle Detection and Electronics (Institute of High Energy Physics, Chinese Academy of Sciences and University of Science and Technology of China)

Abstract: In the past few decades, numerous searches have been made for the neutrinoless double-beta decay (0νββ) process, aiming to establish whether neutrinos are their own antiparticles (Majorana neutrinos), but no 0νββ decay signal has yet been observed. A number of new experiments are proposed but they ultimately suffer from a common problem: the sensitivity may not increase indefinitely with the target mass. We have performed a detailed analysis of the physics potential by using the Jiangmen Underground Neutrino Observatory (JUNO) to improve the sensitivity to 0νββ up to a few meV, a major step forward with respect to the experiments currently being planned. JUNO is a 20 kton low-background liquid scintillator (LS) detector with $3\%/\sqrt{E(\mathrm{MeV})}$ energy resolution, now under construction. It is feasible to build a balloon filled with enriched xenon gas (with ^{136}Xe up to 80%) dissolved in LS, inserted into the central region of the JUNO LS. The energy resolution is ∼1.9% at the Q-value of ^{136}Xe 0νββ decay. Ultra-low background is the key for 0νββ decay searches. Detailed studies of background rates from intrinsic 2νββ and ^{8}B solar neutrinos, natural radioactivity, and cosmogenic radionuclides (including light isotopes and ^{137}Xe) were performed and several muon veto schemes were developed. We find that JUNO has the potential to reach a sensitivity (at 90% C. L.) to $T_{1/2}^{0\nu\beta\beta}$ of 1.8×10^{28} yr (5.6×10^{27} yr) with ∼50 tons (5 tons) of fiducial ^{136}Xe and 5 years exposure, while in the 50-ton case the corresponding sensitivity to the effective neutrino mass, $m_{\beta\beta}$, could reach (5–12) meV, covering completely the allowed region of inverted neutrino mass ordering.

Keywords: double beta decay, liquid scintillator, JUNO

PACS: 23.40.-s, 14.60.Pq, 21.10.Tg **DOI:** 10.1088/1674-1137/41/5/053001

1 Introduction

Currently, the neutrinoless double-beta decay (0νββ) process is the only experimentally feasible and most sensitive way to probe if massive neutrinos are their own antiparticles, namely, Majorana particles. Violation of lepton number is a direct consequence of the 0νββ process, in which a nucleus decays by emitting two electrons and nothing else, $N(A,Z)\to N(A,Z+2)+2\mathrm{e}^-$. Furthermore, searching for 0νββ decay can shed light on the absolute scale of neutrino masses.

Under the standard three neutrino framework, the effective neutrino mass in 0νββ decay is defined as $m_{\beta\beta}\equiv|\sum_i(m_iU_{ei}^2)|$, where U_{ei} (for $i=1,2,3$) denote the matrix elements in the first row of lepton flavor mixing matrix U, and m_i (for $i=1,2,3$) are neutrino masses. For Majorana neutrinos, $m_{\beta\beta}$ is sensitive to the neutrino masses, neutrino mixing angles and Majorana CP phases. Using the standard parametrization of U, $m_{\beta\beta}=|m_1c_{12}^2c_{13}^2\mathrm{e}^{2\mathrm{i}\phi_1}+m_2s_{12}^2c_{13}^2\mathrm{e}^{2\mathrm{i}\phi_2}+m_3s_{13}^2|$ [1], where $c_{12}=\cos\theta_{12}$, $c_{13}=\cos\theta_{13}$, $s_{13}=\sin\theta_{13}$, $s_{12}=\sin\theta_{12}$, $\{\theta_{12},\theta_{13}\}$ are neutrino mixing angles, and $\{\phi_1,\phi_2\}$ are Majorana CP phases. In this definition of $m_{\beta\beta}$, it has been assumed that the 0νββ process is dominated only by the exchange of light Majorana neutrinos. Sterile neutrinos or other exotic physics are not considered. If neutrinos have an inverted mass ordering, $m_{\beta\beta}$ will be greater than ∼0.015 eV, based on current and projected knowledge of the neutrino mixing parameters [2]. For the normal neutrino mass ordering case, no lower bound exists and $m_{\beta\beta}$ could vanish due to the cancellation among the $m_iU_{ei}^2$ terms that are modulated by the Majorana

Received 24 October 2016, Revised 17 January 2017

∗ Supported by Strategic Priority Research Program of Chinese Academy of Sciences(XDA10010900), CAS Center for Excellence in Particle Physics (CCEPP), Postdoctoral Science Foundation of China and Chinese Academy of Sciences (2015IHEPBSH101), Program of International S&T Cooperation of MoST (2015DFG02000)

1) E-mail: zhaojie@ihep.ac.cn

2) E-mail: wenlj@ihep.ac.cn

phases.

Enormous experimental efforts have been made to search for $0\nu\beta\beta$ in the last few decades, using various nuclear isotopes, such as ^{136}Xe, ^{76}Ge, ^{130}Te, etc, as discussed in recent reviews (see [3] and references therein). None of them observed a $0\nu\beta\beta$ decay signal. It is desirable for the next generation $0\nu\beta\beta$ experiments to have a sensitivity of $m_{\beta\beta}$ ~10 meV. With such sensitivity, if the neutrino mass ordering is determined to be inverted by future reactor and accelerator experiments, either a positive (observation of $0\nu\beta\beta$ decay) or a negative (no observation) result would be able to probe the Majorana nature or Dirac nature of neutrinos, respectively.

The half-life of $0\nu\beta\beta$, $T^{0\nu}_{1/2}$, is related to the effective Majorana neutrino mass, $m_{\beta\beta}$, by a phase space factor $G_{0\nu}$ and a nuclear matrix element (NME) $\mathcal{M}_{0\nu}$:

$$(T^{0\nu}_{1/2})^{-1} = G_{0\nu}|\mathcal{M}_{0\nu}|^2 m^2_{\beta\beta} \quad (1)$$

where both $G_{0\nu}$ and $\mathcal{M}_{0\nu}$ can be calculated theoretically. However, the NME has relatively large uncertainties from different nuclear models, see Ref. [4] and references therein.

Two-neutrino double-beta decay ($2\nu\beta\beta$) is allowed by the Standard Model and has been observed in many nuclei. $0\nu\beta\beta$ can be distinguished from $2\nu\beta\beta$ by measuring the sum energy of the two electrons and looking for a mono-energetic peak at the Q-value. The region around the Q-value is referred to as the $0\nu\beta\beta$ window, namely the region of interest (ROI). Different experiments might choose different ROIs, e.g, $\pm1\sigma$, $\pm2\sigma$, $\pm\frac{1}{2}$FWHM or even an asymmetric window around the Q-value, due to different background levels and energy resolutions. Excellent energy resolution and ultra-low background in the ROI are the keys to searching for $0\nu\beta\beta$.

The Jiangmen Underground Neutrino Observatory (JUNO) is a multi-purpose experiment that primarily aims to determine the neutrino mass ordering and to measure precisely the neutrino mixing parameters [2, 5]. Such precision measurement could reduce the range of $T^{0\nu}_{1/2}$ predictions by a factor of 2 [6]. The way to distinguish the neutrino mass ordering at JUNO is via exploring the effect of interference between atmospheric- and solar-Δm^2 driven oscillations [7–9]. The baseline design of the JUNO detector is a 20 kton low-background liquid scintillator (LS) with an unprecedented energy resolution (σ/E) of $3\%/\sqrt{E(\mathrm{MeV})}$. At the Q-value of ^{136}Xe $0\nu\beta\beta$ decay ($Q^{0\nu\beta\beta}$=2457.8 keV), or ^{130}Te ($Q^{0\nu\beta\beta}$=2530 keV), the energy resolution is expected to be ~1.9%, which is suitable for a $0\nu\beta\beta$ search. In addition, online purification is another advantage of LS detectors, and the liquid can reach the adequate level for $0\nu\beta\beta$ searches. KamLAND-Zen [10] and SNO+ [11] are two examples, using ^{136}Xe and ^{130}Te isotopes, respectively. However, their detector sizes are limited so that their sensitivity to $m_{\beta\beta}$ can only reach a few tens of meV. A very large LS detector can perform a better measurement [12].

In this paper, we explore the physics potential of searching for $0\nu\beta\beta$ decays of ^{136}Xe with the JUNO detector, aiming for a few meV sensitivity on $m_{\beta\beta}$, by dissolving enriched pure xenon gas into the liquid scintillator. The Xe-loaded LS target could be separated from the normal LS by deploying a highly transparent and clean balloon. The clean normal LS can provide sufficient passive shielding against external radioactivity, and act as an active zone to track the muons and veto the cosmogenic backgrounds.

2 JUNO detector

The JUNO site has an overburden of ~ 700 m rock. The central detector (CD) is an acrylic sphere of 35.4 m in diameter, holding the 20 kton LS, supported by a spherically latticed shell made of stainless steel (SS) with a diameter of 40.1 m. About ~18000 20-inch PMTs are mounted on the SS latticed shell, looking inward towards the LS target. In addition, up to ~36000 3-inch PMTs will be installed in the gaps between the 20-inch PMTs, to form a complementary calorimetry system and improve the muon measurement. Outside the SS latticed shell, an ultra-pure water pool of 43.5 m diameter and 44 m depth is equipped with ~2000 20-inch PMTs, providing an active cosmic muon veto as a water Cerenkov detector and sufficient passive shielding from the environmental radioactivity. On top of the water pool, the OPERA [13] target trackers are re-used as a complementary Top Tracker system, providing precise track measurement of cosmic muons.

The JUNO LS uses linear alkyl-benzene (LAB) as the solvent, 2,5-diphenyloxazole (PPO) as the primary fluor, and 1,4-bis[2-methylstyryl]benzene (bis-MSB) as the wavelength shifter. The current baseline recipe is adopted from the Daya Bay experiment [14, 15] but without gadolinium doping. As discussed in [2], the baseline LS purity requirement for reactor antineutrino studies is less than 10^{-15} g/g for ^{238}U and ^{232}Th, 10^{-16} g/g for ^{40}K and 1.4×10^{-22} g/g for ^{210}Pb. This is sufficient for the determination of neutrino mass ordering. A sophisticated on-line purification system can be set up, and eventually two orders of magnitude better purity is expected to be achievable. Such optimal purity (10^{-17} g/g for ^{238}U and ^{232}Th, 10^{-18} g/g for ^{40}K and 10^{-24} g/g for ^{210}Pb) is adequate for $0\nu\beta\beta$ searches. The backgrounds caused by the internal impurities are discussed in Section 3.3.

The target element for $0\nu\beta\beta$ searches in this study, as an example, is chosen to be ^{136}Xe for its high purity, high Q-value, and high solubility in LS. Of course other elements are not excluded at present. ^{130}Te is another possible element and has a natural abundance of

34.1%. It is technically challenging to purify tellurium and reach >5% tellurium loading in LAB-based scintillator. As an example, in the Te-loaded phase of the SNO+ experiment, with 0.3% Te-loading, the projected ^{238}U and ^{232}Th concentration would be two orders of magnitude worse than the pure LAB-PPO scintillator [11]. The stability, transparency and light yield would also decrease with high tellurium loading. Unlike xenon, cosmogenic activation of the tellurium nuclei could produce a large number of long-lived radioactive isotopes. To suppress such background, the exposure time of tellurium on the surface should be controlled. A purification process and additional long cooling time underground is necessary [16]. At the depth of JUNO, the cosmogenic background could be serious for $0\nu\beta\beta$ searches. In this study, we choose ^{136}Xe as an example to evaluate the physics potential of the $0\nu\beta\beta$ search at JUNO. The possibility of using ^{130}Te will be evaluated in future.

A transparent and strong balloon can be used to separate the Xe-LS from the normal LS. Xenon gas is found to be soluble into liquid scintillator more than 3% by weight, but the light yield could be reduced depending on the xenon concentration [18]. We expect that such an effect can be compensated by tuning the concentration of the fluors. Thus we assumed 5% by weight of the enriched xenon gas ($^{\rm enr}$Xe) that consists of 80% ^{136}Xe. We chose the ROI as the $\pm\frac{1}{2}$FWHM region around the $Q_{\beta\beta}$ value. The parameters that were chosen in our calculation are compared with the KamLAND-Zen detector in Table 1. The efficiency of $0\nu\beta\beta$ events in the ROI, defined as $\varepsilon_{0\nu\beta\beta}$, was calculated according to the energy resolution at $Q_{\beta\beta}$ and the selected ROI window.

Table 1. Comparison of the parameters of the assumed JUNO Xe-LS detector and KamLAND-Zen detector.

	KamLAND-Zen	JUNO Xe-LS
energy resolution	$6.6\%/\sqrt{E}$ [10]	$3\%/\sqrt{E}$
	$7.3\%/\sqrt{E}$ [17]	
Xe-doping	2.5% (phase I [10])	5%
	2.9% (phase II [17])	
^{136}Xe enrichment	∼91% [10, 17]	80%
$0\nu\beta\beta$ ROI	(2.3, 2.7) MeV [17]	(2403, 2513) keV
$\varepsilon_{0\nu\beta\beta}$ in ROI	89.9%*	75.8%

*corresponding to $\sigma\sim7.3\%\sqrt{E}$ resolution

3 Backgrounds

The natural radioactivity in the liquid scintillator and the long-lived radioactive isotopes produced by muon spallation are the dominant background for the $0\nu\beta\beta$ search. The spallation neutrons produced by cosmic muons can induce the β-decay isotope ^{137}Xe, with a half-life of 3.82 minutes, via the ^{137}Xe(n,γ) reaction. The Q-value for ^{137}Xe decay is 4173±7 keV [19], so the β spectrum overlaps the Q-value of ^{136}Xe $0\nu\beta\beta$ decay. The background rates are evaluated below.

3.1 Intrinsic $2\nu\beta\beta$ background

With finite energy resolution, $2\nu\beta\beta$ events leaking into the $0\nu\beta\beta$ ROI are the intrinsic background. Such background decreases dramatically as energy resolution improves. Hereafter, the background index, defined as the background rate per unit ^{136}Xe mass per ROI, was introduced to quantify the background. We estimated the intrinsic $2\nu\beta\beta$ background rate to be 0.2/ROI/(ton ^{136}Xe)/yr by convoluting the theoretical $2\nu\beta\beta$ energy spectrum [20] with the detector energy resolution curve.

3.2 Solar-ν background

The ν-e scattering signal from ^{8}B solar neutrinos has a continuous spectrum up to >10 MeV, thus it can also contribute to the ROI background. Its signal rate was estimated to be 4.5/kton/day [2]. Using the simulated energy spectrum of the ^{8}B ν-e scattering signal, also described in [2], we estimated the background index to be 28/ROI/(kton Xe-LS)/yr, equivalent to 0.7/ROI/(ton ^{136}Xe)/yr under the assumption of 5% $^{\rm enr}$Xe.

If natural xenon gas is used instead of ^{136}Xe-enriched xenon gas, the background index from the solar neutrinos would be 10 times larger, since the ^{136}Xe abundance in natural xenon is only ∼8%.

3.3 Natural radioactivity

3.3.1 Internal ^{238}U and ^{232}Th contamination

The projected radioactivities of the JUNO detector components such as liquid scintillator, PMT glass, acrylic and supporting structures were discussed in [2, 21]. The external radioactivities could be eliminated by a sufficient fiducial volume cut, e.g, 1 m inward from the LS edge, thus only the internal LS radio-impurities need to be considered. As discussed in Section 2, an optimal radio-purity level $\sim 10^{-17}$ g/g for U and Th is reachable. The following studies are based on this optimal radio-purity assumption.

The β+γ emissions from ^{214}Bi (^{238}U chain, $Q=3.272$ MeV) could be a serious background for $0\nu\beta\beta$ searches, because there is a 2.448 MeV γ line, which can leak into the ROI. From the simulated energy spectra of events from the ^{238}U chain, the background index was calculated to be 8.3/ROI/(ton ^{136}Xe)/yr. The ^{214}Bi-^{214}Po β-α cascade decay ($\tau=237$ μs) is very effective at rejecting ^{214}Bi events. The α energy from ^{214}Po decay is 7.686 MeV, and its quenched response is well above the detector threshold, resulting in a high efficiency of tagging ^{214}Bi events in the ROI. We evaluated the background rejection with Monte Carlo samples by requiring the time

and distance between the prompt β and delayed α decay events to be less than 2.0 ms and 2.0 m, respectively. The residual background is due to the Bi-Po cascade decays that have a decay time longer than 2.0 ms, or occurred within one readout window (nominally 1 μs for JUNO) and their summed energy falls into the ROI. We found ∼99.97% of the events in the ROI from ^{238}U chain were rejected, resulting in <0.003/ROI/(ton ^{136}Xe)/yr residual ROI background.

The fast ^{212}Bi-^{212}Po β-α cascade decay from the ^{232}Th chain ($\tau = 431$ ns) leads to 90% of the two signals occurring in the 1μs nominal readout window. Our GEANT4 MC indicated that the summation of the visible energies of ^{212}Bi $\beta+\gamma$ ($Q = 2.252$ MeV) and ^{212}Po α ($Q = 8.954$ MeV) had a fraction of 6.2% inside the ROI window, while neither the individual β nor α decays could contribute to the ROI. Assuming 10^{-17} g/g ^{232}Th concentration, we estimated the background index from the summation events to be 1.25/ROI/(ton Xe-LS)/yr. Thus, special care should be taken to distinguish and reject these two decays. JUNO will adopt 1 GHz Flash ADC (FADC) to record the full waveforms from all the PMTs inside the readout window, allowing a pulse shape discrimination (PSD) approach to distinguish two decays which are close in time. The LAB-based liquid scintillator was demonstrated to have good capability of e^-/α discrimination [22]. A full MC simulation including scintillation processes and PMT timing resolution was performed for the decays. We developed a PSD method by using the width and the tail fraction of the measured scintillation time profile, in which the time-of-light of photons were corrected. The discrimination efficiency was found to reach >97.5%, resulting in a residual ROI background of 0.03/ROI/(ton ^{136}Xe)/yr. Our GEANT4 MC indicated negligible contribution from internal ^{208}Tl decays ($Q = 4.999$ MeV) to the ROI, because the visible energy inside the LS is the summation of the β and γ energies, which has a minimum energy of 3.2 MeV. This is different from the surface contamination, where βs deposit their energy in the vessel material without scintillation, but the 2.615 MeV γs could leak into the ROI.

For comparison, the ^{238}U and ^{232}Th contamination in Borexino LS detector reached $<10^{-18}$ g/g [23], while the radio-purity in KamLAND-Zen detector is $\sim 3.5\times10^{-16}$ g/g for ^{238}U and $\sim 2.2\times10^{-15}$ g/g for ^{232}Th, respectively [10]. Past experiences in LS purification would benefit JUNO to reach its radio-purity goal.

3.3.2 External radioactivity

As discussed in Section 2, a highly transparent balloon can be used to contain the Xe-LS. Although the balloon material could be very radio-pure (e.g, ppt level), the possible dust contamination during installation and the radon contamination during LS purification could yield much higher ^{214}Bi levels on the surface of the balloon. A fiducial volume cut is effective against ^{214}Bi and ^{208}Tl decays from the balloon. We consider that a 1 m cut from the Xe-LS target edge would be sufficient.

Extreme care should be taken to prevent radon (mainly ^{222}Rn , $\tau = 5.52$ day) from penetrating into the Xe-LS during the purification process. We put a requirement of 5×10^3 atoms/(kton Xe-LS)/yr external radon leakage rate. Taking into account the 99.97% rejection efficiency via ^{214}Bi-^{214}Po tagging, it would lead to a 0.2/ROI/(ton ^{136}Xe)/yr background rate.

3.4 Cosmogenic backgrounds

Energetic cosmic muons can cause spallation in organic liquid scintillator, and produce long-lived radioactive isotopes via the photon-nuclear or hadronic processes. The overburden for the JUNO detector is 748 m, and the muon flux at the JUNO site is about 0.003 Hz/m^2, which is a factor of ∼2 more than the underground lab at Kamioka. The rate of muons passing through the JUNO LS volume is about 3.0 Hz, with a mean energy of 215 GeV.

Table 2. Summary of the simulated muon-induced radioactive isotopes (mostly with $Z \leqslant 6$) in the JUNO LS. Only the isotopes that can contribute to the $0\nu\beta\beta$ window are listed. ^{10}C, ^{6}He, ^{8}Li and ^{12}B are the four dominant contributors, while the contributions from other isotopes are combined, such as ^{11}Be ($\tau_{1/2}$ =13.8 s, $Q(\beta^-) = 11.5$ MeV), ^{9}C ($\tau_{1/2} = 0.13$ s, $Q(\beta^+) = 16.5$ MeV), ^{16}N ($\tau_{1/2} = 7.13$ s, $Q(\beta^-\gamma) = 10.4$ MeV), ^{9}Li ($\tau_{1/2} = 0.178$ s, $Q(\beta^-\gamma\text{-n}) = 13.6$ MeV), ^{8}He ($\tau_{1/2} = 0.12$ s, $Q(\beta^-\gamma\text{-n}) = 10.7$ MeV). The latter two isotopes are β-n emitters with branching ratios of 51% and 16%, respectively. Such β-n decays can be rejected by coincidence cuts and were removed in this table.

	$T_{1/2}$ in JUNO LS	radiation E/ MeV	$R_{\rm prod}$/(ton^a·yr)$^{-1}$ FLUKA [2]	this work	primary process	accompanied neutrons 0n	1n	2n	3n	background Index /(ROI·ton^b·yr)$^{-1}$
^{10}C	19.3 s	3.65 ($\beta^+\gamma$)	9.8	9.3	π^+ Inelastic	2.20%	37.4%	38.3%	22.1%	16.4
^{6}He	0.807 s	3.51 (β^-)	11.0	6.1	n Inelastic	39%	42.7%	10.5%	6.7%	8.8-4.9
^{8}Li	0.84 s	16.0 ($\beta^-\alpha$)	19.0	8.4	n Inelastic	62.8%	19.2%	16.3%	1.5%	3.4-1.5
^{12}B	0.02 s	13.4 (β^-)	19.6	12.4	n Inelastic	93.6%	6.3%	<0.1%	—	3.0-1.9
others	—	—	2.5	0.81	—	—	—	—	—	0.51

[a] here ton is a unit of Xe-LS mass

[b] here ton is a unit of ^{136}Xe mass

The production of the radioactive isotopes in JUNO LS was evaluated by GEANT4 [24] simulation. A Monte Carlo (MC) muon data set of ∼342 days' worth of statistics was produced to study the cosmogenic backgrounds in the $0\nu\beta\beta$ search. The results are summarized in Table 2, including the raw production rates, the primary production processes, the fractions for different number of accompanied neutrons and the background indexes in the ROI. The production rates from the earlier analysis [2] using FLUKA [25] were also listed for comparison. Both GEANT4 and FLUKA indicate that ^{10}C, ^{6}He, ^{8}Li and ^{12}B are the dominant contributors. Other isotopes were found to have relatively small contributions in the ROI, thus they were combined in the last row of the table. Given their long half-lives and relatively high muon rate in the JUNO detector, it was challenging to reject those backgrounds. In Table 2, our GEANT4 MC predicted a similar ^{10}C production yield to FLUKA, whereas it gave a lower ^{6}He, ^{8}Li and ^{12}B production yield than FLUKA. This is probably due to different hadronic interaction models being used. In the following analysis we used the newly produced GEANT4 MC data with large statistics, showing that the residual cosmogenic backgrounds after muon veto is evaluated to be ∼10% of the total background. Thus the differences between FLUKA and GEANT4 were considered not to affect the main conclusion of this paper. To mimic a real data set, we assigned a time stamp for each primary muon and its daughters according to the average R_μ=3 Hz muon rate, then the primary muons and their subsequent events were mixed and sorted.

Cosmogenic isotopes are mainly produced by energetic showering processes in the LS. Table 2 shows that ∼98% of ^{10}C, ∼60% of ^{6}He and ∼37% of ^{8}Li are accompanied by $\geqslant$1 neutrons, allowing us to develop a special veto strategy to reject those β-decays. Although the ^{12}B production has weak correlation with neutrons, it has a relatively short half-life and thus can be efficiently rejected by vetoing a longer time. The veto methods to reject the cosmogenic backgrounds and the results are discussed in following subsections.

The previous measurements [26] and simulations [27], as well as our simulation show that the distance from the isotope's production position to its parent muon track approximately follows an exponential profile. Thus, vetoing a cylindrical volume along the reconstructed muon track for sufficient time can significantly reduce the muon induced backgrounds.

As described in Section 2, the JUNO central detector will be equipped with a vast number of 3-inch PMTs, providing excellent track reconstruction for both minimum ionizing muons and showering muons. However, the track reconstruction of a showering muon is non-trivial. Our simulation indicated that a muon changes little in its direction after producing a shower. Thus the entry and exit points in the pattern of hit PMTs can give a good estimation of the muon track. In addition, we found that high multiplicity neutrons were produced near the high $\mathrm{d}E/\mathrm{d}x$ region, and those neutrons' vertices could be used to further constrain the muon track and reconstruct the location of the muon shower.

The muon events were first categorized into two types: the normal muons ($\mu_{\rm norm}$) and the neutron-associated muons ($\mu_{\rm n-assoc}$). Their identification and corresponding veto criteria are described below:

1) $\mu_{\rm norm}$ identification: if the distance from the LS center to the muon track is within ($R_{\rm Xe}$+3) meters, where $R_{\rm Xe}$ is the radius of Xe-LS volume. $\mu_{\rm norm}$ veto: any signal within a veto time window of 1.2 s and within a 3 m cylinder along the muon track was rejected.

2) $\mu_{\rm n-assoc}$ identification: among the $\mu_{\rm norm}$ samples, if a neutron-like signal occurs within 1 ms after the muon and within $(R_{\rm Xe}+2)$ meters from the detector center. The neutron-like signal is identified as an event in the n-capture energy window, (2.0, 2.4) MeV.

$\mu_{\rm n-assoc}$ veto: any signal within 2 meters from each associated neutron-like signal and within a veto time window of $t^{\rm veto}_{n-\mu}$ was rejected.

We evaluated the efficiency of the muon veto and the residual cosmogenic background for different target radii R_{Xe}. For each assumed $R_{\rm Xe}$, the muons were first categorized according to the above criteria. By definition, the rates of $\mu_{\rm norm}$ and $\mu_{\rm n-assoc}$ depend on the Xe-LS target size $R_{\rm Xe}$. With the MC data set, the rates were parameterized as $R^{\rm norm}_{\mu} = 9.38\times10^{-3}\cdot(R_{\rm Xe}+3)^2$ Hz and $R^{\rm n-assoc}_{\mu} = 3.58\times10^{-5}\cdot(R_{\rm Xe}+2)^3$ Hz, respectively. Then we applied the above muon veto strategies to the mixed MC data set, and particularly tested different values of the veto window $t^{\rm veto}_{n-\mu}$. Finally the live time and the rate of residual background were calculated.

3.4.1 Long-lived light isotopes

Among the dominant isotope backgrounds, ^{10}C has the longest half-life $\tau(^{10}\mathrm{C}) = 27.8$ s, thus the veto window $t^{\rm veto}_{n-\mu}$ should be sufficiently long to reject ^{10}C and ^{6}He effectively. We tested different $t^{\rm veto}_{n-\mu}$: $2\tau(^{10}\mathrm{C})$, $4\tau(^{10}\mathrm{C})$ and $6\tau(^{10}\mathrm{C})$, as shown in Table 3.

Increasing $t^{\rm veto}_{n-\mu}$ significantly reduced the ^{10}C and ^{6}He rates, with negligible loss of live-time due to the low rate of $\mu_{\rm n-assoc}$. When using the $\mu_{\rm norm}$ veto plus $6\tau(^{10}\mathrm{C})$ window for $\mu_{\rm n-assoc}$ veto, the reduction factors for ^{10}C and ^{6}He were 309 and 78, respectively. Although the MC indicated that the ^{12}B production had a weak correlation with the neutron production, it was also strongly suppressed after applying the above muon veto, due to a much shorter half-life. Table 3 showed that with a proper muon veto the cosmogenic backgrounds could be well controlled.

To estimate the veto efficiency, tracer events that

were uniformly distributed in time and within the LS volume were mixed into the sorted MC data set. After applying the selections cuts, the efficiency was estimated as M_s/M, where M was the total number of tracer events and M_s was the number of tracer events that survived the veto. The efficiency was precisely calculated with large statistics of the tracer events. In Table 3, the efficiency varied a little when adding the $\mu_{n-assoc}$ veto. In addition, we found the efficiency and the background index slightly changed for different Xe-LS target sizes R_{Xe}. The last column in the table was used for sensitivity calculation.

Table 3. Background indices of the muon-induced radioactive isotopes, for different muon veto schemes. The values are based on GEANT4 simulation. ^{10}C, ^{6}He, ^{8}Li and ^{12}B are the four dominant contributors to the ROI background, while the contribution from other isotopes are combined. Taking the FLUKA results from Table 2, the total residual background would increase to 0.21/ROI/(ton ^{136}Xe)/yr after μ_{norm} veto plus $\mu_{n-assoc}$ veto with $t^{veto}_{n-\mu}=6\tau(^{10}C)$.

	background index[a]				
	no veto	μ_{norm} veto	n-associated muon veto		
			2 $\tau_{^{10}C}$	4 $\tau_{^{10}C}$	6 $\tau_{^{10}C}$
efficiency ε_μ	1	0.902	0.879	0.858	0.837
^{10}C	16.4	14.3	1.98	0.27	0.053
^{6}He	4.9	1.69	0.065	0.065	0.063
^{8}Li	1.5	0.54	0.017	0.017	0.016
^{12}B	1.9	0.05	3.8e-4	3.8e-4	3.8e-4
others	0.51	0.17	0.01	0.01	0.01
total bkg	25.2	16.8	2.1	0.36	0.14

[a] in /ROI/(ton ^{136}Xe)/yr unit

3.4.2 ^{137}Xe background

The neutrons that are produced by the cosmic muons can thermalize via collision with the nuclei in the LS, then finally get captured on a nuclide. ^{136}Xe can capture the thermal neutrons and produce radionuclide ^{137}Xe via the ^{136}Xe(n,γ) process, although the probability is small. ^{137}Xe atoms are produced in a capture state with the excited state energy of 4025.46±0.27 keV [28], then deexcite into the ground state promptly, primarily through γ emission. The ground state of ^{137}Xe then purely β^- decays (τ = 5.51 min, $Q = 4173 \pm 7$ keV), resulting in contamination of the ROI.

Similar to ^{10}C and ^{6}He, the ^{136}Xe(n,γ)^{137}Xe cascade also provides a nice triple-coincidence signature of the muon, the neutron capture on ^{136}Xe and the subsequent ^{137}Xe decay, to identify and reject such muon-induced ^{137}Xe background. The neutron capture on ^{137}Xe is easy to identify due to a much higher energy than the natural radioactivity.

The ^{137}Xe production was estimated from the neutron capture process in the Xe-LS, as shown in Table 4. The expected neutron capture fractions on protons, ^{10}C, ^{136}Xe and ^{134}Xe in the KamLAND-Zen Xe-LS were reported as 0.994, 0.006, 9.5×10^{-4} and 9.4×10^{-5}, respectively [29]. In Section 2, we considered doping 5% by weight of ^{enr}Xe with 80% ^{136}Xe into the JUNO LS, thus the neutron capture fraction on ^{136}Xe is expected to be $\sim 1.7\times10^{-3}$. Since KamLAND-Zen observed a ∼13% increase in the spallation neutron flux in the Xe-LS relative to the normal LS [10], thus a factor of 1.13 was taken into account when estimating the neutron rate in JUNO Xe-LS. In addition, our ROI region is a factor of 4 narrower than KamLAND-Zen due to better energy resolution, as shown in Table 1. Finally the background index from ^{137}Xe was calculated to be 2.3/ROI/(ton ^{136}Xe)/yr.

Similar to the $\mu_{n-assoc}$ veto, we can develop ^{137}Xe-associated muon ($\mu_{Xe-assoc}$) veto criteria:

- $\mu_{Xe-assoc}$ identification: among the μ_{norm} samples, if a n-^{136}Xe capture candidate occurs within 1 ms after a muon and within (R_{Xe}+1) meters from the detector center.

  $\mu_{Xe-assoc}$ veto: any signal within 1 meter of each associated n-^{136}Xe signature and within a veto time window of $5\tau(^{137}Xe)$ was rejected.

A FLUKA simulation with the EXO-200 detector showed that thermal neutron capture was the absolute dominant production process for ^{137}Xe [30]. Our GEANT4 simulation with Xe-LS gave consistent results. After applying the above veto scheme to the GEANT4 MC data set, the residual ^{137}Xe β-decay was 0.07/ROI/(ton ^{136}Xe)/yr.

Table 4. The estimated ^{137}Xe production rate via ^{136}Xe(n,γ) process in the assumed JUNO Xe-LS detector, which was scaled from the KamLAND-Zen detector.

	KamLAND-Zen	JUNO Xe-LS
R_n in Xe-LS[a]	0.045 [26]	0.073 [2]
n-^{136}Xe fraction	9.5×10^{-4} [10, 29]	1.7×10^{-3}
^{136}Xe(n,γ)^{137}Xe yield[b]	61	98
background index[c]	8.2	2.3

[a] in Hz/(kton Xe-LS) unit
[b] in (ton ^{136}Xe)$^{-1}$·yr^{-1} unit
[c] in ROI^{-1}·(ton ^{136}Xe)$^{-1}$·yr^{-1} unit

3.5 Background summary

The ROI backgrounds are summarized in Table 5. We evaluated the total background index for various Xe-LS target sizes, and with little difference. Other backgrounds, such as (α,n) reactions, were also evaluated and found to be much less than the components in Table 5. The reduction of the cosmogenic backgrounds in each muon veto step is shown in Fig. 1.

Table 5. Summary of the projected backgrounds in the 0νββ ROI. For light cosmogenic isotopes, the values are from GEANT4 MC, while for FLUKA MC the total residual background would increase 0.07/ROI/(ton ^{136}Xe)/yr.

summary of backgrounds in 0νββ ROI [ROI·(ton ^{136}Xe)·yr]$^{-1}$	
2νββ	0.2
^{8}B solar ν	0.7
cosmogenic background	
^{10}C	0.053
^{6}He	0.063
^{8}Li	0.016
^{12}B	3.8×10^{-4}
others ($Z\leqslant6$)	0.01
^{137}Xe	0.07
internal LS radio-purity (10^{-17} g/g)	
^{214}Bi (^{238}U chain)	0.003
^{208}Tl (^{232}Th chain)	—
^{212}Bi (^{232}Th chain)	0.03
external contamination	
^{214}Bi (Rn daughter)	0.2
total	1.35

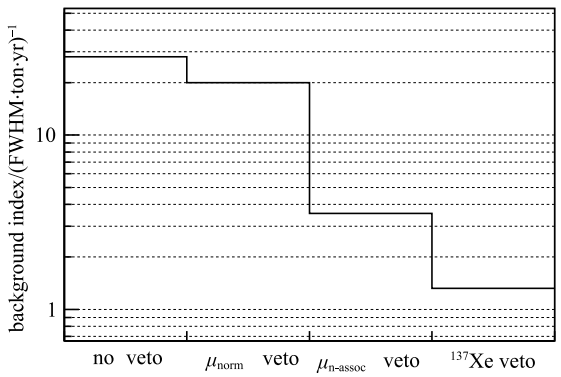

Fig. 1. The reduction of the total background index for different muon veto schemes. The $\mu_{\rm norm}$ and $\mu_{\rm n-assoc}$ refer to the normal muon veto and the neutron-associated muon veto methods, respectively, as described in Section 3.4.

4 Sensitivity

In an experiment that searches for rare decays, with certain projected backgrounds and no true signal, the sensitivity $S(b)$ can be given by $S(b) = \sum_{n=0}^{\infty} P(n|b)U(n|b)$ [31], where $P(n|b)$ is a Poisson $p.d.f$ for the background fluctuation, and $U(n|b)$ is a function yielding the upper limit at the desired C. L. for a given observation n and a mean projected background level b. In a real 0νββ experiment with non-negligible background, the sensitivity of the 0νββ half-life can be calculated as

$$T_{1/2}^{0\nu\beta\beta} = \ln 2 \cdot \frac{N_A}{M_{\rm isotope}} \cdot \frac{M\cdot\epsilon\eta\cdot t}{\alpha\cdot\sqrt{b}} \qquad (2)$$

where $N_A = 6.022\times10^{23}$ is Avogadro's constant, $M_{\rm isotope}$ is the molar mass of the 0νββ decay isotope, M is the fiducial target mass, t is the live time (the product $M\cdot t$ is usually referred to as the total exposure), ϵ is the detection efficiency, and η is the abundance of the 0νββ isotope. In the calculation, the efficiency ϵ included the energy cut efficiency of the 0νββ ROI in Table 1 and the efficiency of the muon veto in Table 3, and the combined efficiency is listed in Table 6. Depending on whether 90% or 95% C. L. is quoted, α is 1.64 or 1.96, respectively.

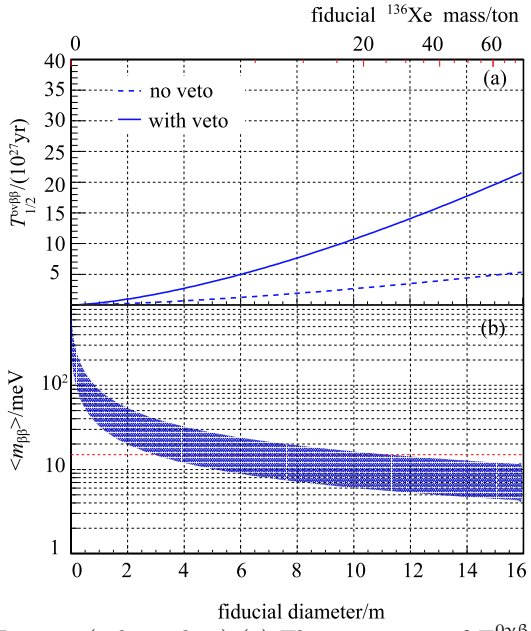

Fig. 2. (color online) (a) The sensitivity of $T_{1/2}^{0\nu\beta\beta}$ versus the JUNO Xe-LS volume size and fiducial ^{136}Xe mass assuming 5 years livetime. The two curves represent the case w/o and w/ muon veto, respectively, and the latter is used to calculate the $m_{\beta\beta}$ sensitivity. (b) The sensitivity of effective neutrino mass $m_{\beta\beta}$. The uncertainty band is due to different NME models (EDF [32], ISM [33], IBM-2 [34], Skyrme QRPA [35], QRPA [36]). The red dashed line corresponds to 15 meV.

Given that the JUNO detector has 20 kton LS, it has the capability for a large Xe-LS volume. The sensitivities of $T_{1/2}^{0\nu\beta\beta}$ and corresponding effective neutrino mass $m_{\beta\beta}$ versus different Xe-LS volume size and fiducial ^{136}Xe mass are shown in Fig. 2. The uncertainty band of $m_{\beta\beta}$ accounts for different NME models [32–36]. Assuming ∼50 tons of ^{136}Xe and 5 years live time,

the projected $T_{1/2}^{0\nu\beta\beta}$ sensitivity (90% C.L) could reach $\sim 1.8\times10^{28}$ yr with a sophisticated muon veto scheme, which is a factor of 4 better than the no veto case. This allows probing of $m_{\beta\beta}$ down to (5–12) meV, completely below the region allowed by the inverted neutrino mass ordering scenario. We understand that the cost of producing 50 tons enriched xenon is currently practically unacceptable, however, to demonstrate that the sensitivity could really scale with target mass, we quote a large target mass.

The sensitivity for a more realistic scenario, with 5 tons of ^{136}Xe and 5 years live time, is superimposed in Fig. 3. The projected $T_{1/2}^{0\nu\beta\beta}$ sensitivity (90% C.L) would be $\sim 5.6\times10^{27}$ yr. We also would like to point out that, since M in Eq. (2) refers to the fiducial target mass, the fiducial cut efficiency was automatically included. As discussed in Section 3.3.2, a 1-m cut from the Xe-LS target edge was considered, thus the fiducial efficiency was 45% and 67% for 5 tons and 50 tons of ^{136}Xe, respectively. In future work, we expect to perform a 2D fit simultaneously to the energy spectra and stand-off distance, which is defined as the distance from the event position to the Xe-LS edge, in order to enlarge the fiducial volume and improve the sensitivity.

Table 6. A comparison of current and future $0\nu\beta\beta$ experiments, including: the target $0\nu\beta\beta$ isotope and its abundance in the natural isotopes; the exposure of the $0\nu\beta\beta$ isotope; the detection efficiency for $0\nu\beta\beta$; the background index (B.I.); the 90% C.L. limit or sensitivity of $0\nu\beta\beta$ decay half-life $T_{1/2}^{0\nu}$; and the 90% C.L. limit or sensitivity of the effective neutrino mass $m_{\beta\beta}$. Unless specially noted, the background index, in events/(keV ton yr) unit, is defined as the background counts normalized by the ROI width and the $0\nu\beta\beta$ isotope exposure.

experiment	isotope	exposure /(ton·yr)	$\varepsilon_{0\nu\beta\beta}$	B.I.	ROI /keV	90% C.L. limit (L) or sensitivity (S)	
						$T_{1/2}^{0\nu}$, $\times10^{27}$yr	$m_{\beta\beta}$/meV
current results							
CUORE-0 [37]	^{130}Te (34.17%)	9.8e-3	0.813	58[a]	5.1 FWHM	0.004[b] (L)	270 − 760 (L)
EXO-200 [38]	^{136}Xe (80.6%)	0.1	0.846	1.7[c]	150 (2σ)	0.019 (S)	190 − 450 (L)
GERDA [39]	^{76}Ge (87%)	5e-3[d]	0.51	3.5	10.2 (3σ)	0.04[e] (S)	160 − 260 (L)
(phase-II)		5.8e-3	0.60	0.7	7.7 (3σ)		
KamLAND-Zen [17]	^{136}Xe (90.77%)	∼0.255	—	28.1/yr	400	0.056 (S), 0.092 (L)	61 − 165 (L)[f]
(phase-II)		∼0.249	—	15.5/yr	400		
prospective sensitivities							
EXO-200 phase-II [40]	^{136}Xe	∼0.16 · 3	—	—	—	0.057 (S)	110 − 260 (S)
KamLAND-Zen 800 [17]	^{136}Xe	∼0.8 · ?	—	—	—	—	∼50 (S)
SNO+ phase I [11]	^{130}Te	∼0.8 · 5	—	13.4/yr	—	0.09 (S)	55 − 133 (S)
CUORE [41]	^{130}Te	0.206 · ?	—	10	—	0.095 (S)	50 − 130 (S)
GERDA Phase-II [39]	^{76}Ge	>0.1	—	∼1	—	>0.1 (S)	—
SNO+ Phase II [11]	^{130}Te	∼8.0 · ?	—	—	—	0.7 (S)	19 − 46 (S)
KamLAND2-Zen [42]	^{136}Xe	∼1 · ?	—	—	—	—	∼20 (S)
nEXO [43]	^{136}Xe (90%)	∼5 · 5	—	0.02[g]	58$^{\rm FWHM}$	6.6 (S)	7 − 22 (S)
JUNO Xe-LS	^{136}Xe (80%)	50 · 5	0.63	0.012	110$^{\rm FWHM}$	18 (S)	5 − 12 (S)

[a] The quoted B.I. is normalized to the total TeO_2 exposure (35.2 kg yr). The same for CUORE.
[b] This limit is from the combination with the 19.75 kg·yr exposure of ^{130}Te from Cuoricino, while it is 2.7×10^{24} yr for CUORE-0 only.
[c] This quoted B.I. is normalized to the total Xe exposure (123.7 kg yr).
[d] The quoted 5 (5.8) kg·yr exposure is for the total coaxial (BEGe) detectors in GERDA Phase-II.
[e] The limits of $T_{1/2}^{0\nu}$ and $m_{\beta\beta}$ are from the combination of Phase-I and Phase-II. For Phase-I only, it was 2.1×10^{25} yr (90% C. L.).
[f] The quoted limit is from the combination of KamLAND-Zen Phase-I and Phase-II.
[g] The quoted B.I. is for the inner 3-ton xenon mass.

5 Summary and discussion

In this work, we explored the physics potential of a $0\nu\beta\beta$ search with the JUNO detector via dissolving ^{136}Xe-enriched xenon gas into LS. JUNO is designed to achieve $3\%/\sqrt{E(\rm MeV)}$ energy resolution for determining neutrino mass ordering, thus the energy resolution at ^{136}Xe $Q_{\beta\beta}$ is expected to be 1.9%, resulting in relatively small intrinsic $2\nu\beta\beta$ background in the ROI. We performed detailed analyses of other ROI backgrounds from ^{8}B solar ν-e scattering events, LS natural radioactivity, muon induced radionuclides, and so on. An optimal

purity (10^{-17} g/g for ^{238}U and ^{232}Th) is assumed with proper LS on-line purification. A sophisticated muon veto scheme using the correlation between the spallation neutrons and the isotopes was developed to reject the long-lived cosmogenic backgrounds. Eventually a low background rate of ~1.35/ROI/(ton ^{136}Xe)/yr was expected to be achievable. Assuming 5 tons of fiducial ^{136}Xe target mass and 5 years live time, we projected the 90% C.L sensitivity of $T_{1/2}^{0\nu\beta\beta}$ (or $m_{\beta\beta}$) to be $\sim 5.6\times10^{27}$ yr (or 8–22 meV). In the case of 50 tons of fiducial ^{136}Xe, the 90% C.L sensitivity of $m_{\beta\beta}$ can scale up to (5–12 meV), which is well below the region allowed by the scenario of inverted neutrino mass ordering.

Ultra-low background and excellent energy resolution are the two critical factors for the next generation $0\nu\beta\beta$ experiments. Table 6 summarizes the current experimental results or the projected sensitivities of CUORE [37, 41], EXO-200 [38], GERDA [39], KamLAND-Zen [17], SNO+ [11], nEXO [40, 43], as well as the potential Xe-LS detector at JUNO. Different experiments use different definitions when reporting the background rate, as well as choosing different $0\nu\beta\beta$ windows. In order to compare different experiments, we rewrite the sensitivity formula Eq. 2 as

$$\left(\frac{T_{1/2}^{0\nu\beta\beta}\cdot\alpha}{\ln 2\cdot N_A}\right)^2 = \frac{M_{\rm norm}}{B_{\rm I}} \qquad (3)$$

where $B_{\rm I} = \dfrac{b}{(M\epsilon\eta\cdot t/M_{\rm isotope})\cdot{\rm ROI}}$ is the redefined background index, and $M_{\rm norm} = \dfrac{M\epsilon\eta\cdot t}{{\rm ROI}\cdot M_{\rm isotope}}$ is the normalized detector exposure.

With the new definition, Fig. 3 shows a comparison of the experiments listed in Table 6. The dashed lines represent the contours of different sensitivities of $T_{1/2}^{0\nu\beta\beta}$ using Eq. (3). The data points roughly agree but do not exactly align with the calculated contours, because different experiments have different systematics and use different fitting or statistical analysis methods. Fig. 3 also indicates that the next generation $0\nu\beta\beta$ experiments should pursue both ultra-low background and very large detector exposure.

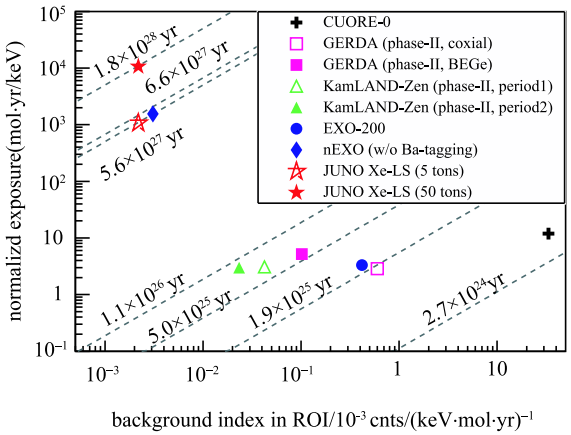

Fig. 3. (color online) The re-defined background indices and detector exposures in the ROIs of CUORE-0 [37], GERDA Phase-II [39], KamLAND-Zen [17], EXO-200 [38], nEXO [40] and the potential Xe-LS detector at JUNO. The dashed lines are the contours of different sensitivities.

References

1 J. Zhang and S. Zhou, Phys. Rev. D, **93** (1): 016008 (2016)
2 F. An et al (JUNO Collaboration), J. Phys. G, **43** (3): 030401 (2016)
3 I. Ostrovskiy and K. O'Sullivan, Mod. Phys. Lett. A, **31** (18): 1630017 (2016)
4 J. Engel, J. Phys. G, **42** (3): 034017 (2015)
5 Z. Djurcic et al (JUNO Collaboration), arXiv:1508.07166 [physics.ins-det]
6 S. F. Ge and W. Rodejohann, Phys. Rev. D, **92** (9): 093006 (2015) doi:10.1103/PhysRevD.92.093006 [arXiv:1507.05514 [hep-ph]]
7 L. Zhan, Y. Wang, J. Cao, and L. Wen, Phys. Rev. D, **78**: 111103 (2008) doi:10.1103/PhysRevD.78.111103 [arXiv:0807.3203 [hep-ex]]
8 L. Zhan, Y. Wang, J. Cao, and L. Wen, Phys. Rev. D, **79**: 073007 (2009) doi:10.1103/PhysRevD.79.073007 [arXiv:0901.2976 [hep-ex]]
9 Y. F. Li, J. Cao, Y. Wang, and L. Zhan, Phys. Rev. D, **88**: 013008 (2013) doi:10.1103/PhysRevD.88.013008 [arXiv:1303.6733 [hep-ex]]
10 A. Gando et al (KamLAND-Zen Collaboration), Phys. Rev. C, **85**: 045504 (2012)
11 S. Andringa et al (SNO+ Collaboration), Adv. High Energy Phys., **2016**: 6194250 (2016)
12 D. E. Jaffe, Phys. Procedia, **61**: 319 (2015) doi:10.1016/j.phpro.2014.12.051
13 R. Acquafredda et al, JINST, **4**: P04018 (2009)
14 Y. Y Ding, J. C. Liu, Z. M. Wang, Z. Y. Zhang, P. J. Zhou, and Y. L. Zhao, Nucl. Instrum. Meth. A, **584**: 238 (2008)
15 W. Beriguete et al, Nucl. Instrum. Meth. A, **763**: 82 (2014)
16 V. Lozza and J. Petzoldt, Astropart. Phys., **61**: 62 (2015)
17 A. Gando et al (KamLAND-Zen Collaboration), Phys. Rev. Lett., **117** (8): 082503 (2016), Phys. Rev. Lett. **117** (10): 109903 (2016)
18 Yoshihito Gando, Present Status of KamLAND-Zen, talk on International Workshop on Double Beta Decay and Neutrinos, Nov, 2011
19 E. Browne and J.K. Tuli. Nuclear data sheets for $a = 137$, Nuclear Data Sheets, **108** (10): 2173–2318(2007)
20 G. K. Schenter and P. Vogel, Nucl. Sci. Eng., **83**: 393 (1983)
21 X. Y. Li, Z. Y. Deng, L. J. Wen, W. D. Li, Z. Y. You, C. X. Yu, Y. M. Zhang, and T. Lin, Chin. Phys. C, **40** (2): 026001 (2016)
22 X. B. Li et al, Chin. Phys. C, **35**(11): 1026, 2011
23 G. Bellini et al (BOREXINO Collaboration), Nature, **512** (7515): 383 (2014)

24 S. Agostinelli et al (GEANT4 Collaboration), Nucl. Instrum. Methods A, **506**: 250 (2003)
25 A. Ferrari, P. R. Sala, A. Fasso, and J. Ranft, CERN-2005-010, SLAC-R-773, INFN-TC-05-11
26 S. Abe et al (KamLAND Collaboration), Phys. Rev. C, **81**: 025807 (2010)
27 S. W. Li and J. F. Beacom, Phys. Rev. D, **92** (10): 105033 (2015)
28 S. Mughabghab, http://www.nndc.bnl.gov/atlas/
29 K. Asakura et al (KamLAND-Zen Collaboration), Nucl. Phys. A, **946**: 171 (2016)
30 J. B. Albert et al (EXO-200 Collaboration), JCAP, **1604** (04): 029 (2016)
31 J. J. Gomez-Cadenas, J. Martin-Albo, M. Sorel, P. Ferrario, F. Monrabal, J. Munoz-Vidal, P. Novella, and A. Poves, JCAP, **1106**: 007 (2011)
32 T. R. Rodriguez and G. Martinez-Pinedo, Phys. Rev. Lett., **105**: 252503 (2010)
33 J. Menendez, A. Poves, E. Caurier, and F. Nowacki, Nucl. Phys. A, **818**, 139 (2009)
34 J. Barea, J. Kotila, and F. Iachello, Phys. Rev. C, **91** (3): 034304 (2015)
35 M. T. Mustonen and J. Engel, Phys. Rev. C, **87** (6): 064302 (2013)
36 J. Engel, F. Simkovic and P. Vogel, Phys. Rev. C, **89** (6) 064308 (2014)
37 K. Alfonso et al (CUORE Collaboration), Phys. Rev. Lett., **115** (10): 102502 (2015)
38 J. B. Albert et al (EXO-200 Collaboration), Nature, **510**: 229 (2014)
39 Matteo Agostini, First Results from GERDA Phase II, talk at NEUTRINO 2016
40 Liang Yang, Status and Prospects for the EXO-200 and nEXO Experiments, talk at NEUTRINO 2016
41 Lucia Canonica, Status and Prospects for CUORE, talk at NEUTRINO 2016
42 Junpei Shirai, Results and Future Plans for the KamLAND-Zen, talk at NEUTRINO 2016
43 Yi-Hsuan Lin, nEXO: the next Generation Neutrinoless Double Beta Decay ($0\nu\beta\beta$) Search, talk at APS April Meeting 2015